ASTRONOMY & ASTROPHYSICS
SUPPLEMENT SERIES

Astron. Astrophys. Suppl. Ser. **113,** 1-19 (1995)

The ultraviolet spectrum of η Carinae. II. 1980 IUE observations of the Homunculus*

G.B. Baratta[1], A. Cassatella[2] and R. Viotti[2]

[1] Osservatorio Astronomico, Via del Parco Mellini 84, I-00136 Roma, Italy
baratta@oarhp1.rm.astro.it
[2] Istituto di Astrofisica Spaziale, CNR, Via E. Fermi 21, I-00044 Frascati RM, Italy
cassatella, viotti@alpha1.ias.fra.cnr.it

Received February 5, 1994; accepted March 21, 1995

Abstract. — We analyze the ultraviolet observations of the circumstellar nebula of η Car (the *Homunculus*) obtained in December 1980 with IUE. A high resolution spectrum was obtained with the IUE large aperture from 6″ to 17″NW of η Car, near the H condensation (the *head*). The measured flux appears two orders of magnitude larger than that expected from the instrumentally scattered light (stray light). The high resolution 2295 to 3200 Å spectrum of the nebula is given in the form of Atlas to provide a quantitative ground for a detailed comparison with the UV spectrum of the stellar core discussed by Viotti et al. (1989). The terminal velocities of the P Cygni absorption components are similar in the stellar core and in the nebula, but the blue side of the emission appears less absorbed in the latter. The high excitation Fe II emission lines, such as the 2507−08 Å blend, appear sharp and very prominent in emission. A terminal velocity of $\geq$1000 km s^{-1} is derived from the analysis of the stellar and nebular Mg II doublet. We have also identified Fe I emission lines at 2823 and 2844 Å which are fluorescence excited by the Mg II *k* line. The low resolution IUE spectrum of the condensations H (8″NW of η Car), D (5″E) and S (11″SW), is also analyzed, and the spatial physical structure of the nebula near D and S is discussed. The long-wave spectrum is dominated by broad emission blends of Fe II and Mg II. The short-wave spectrum of the X-ray emitting S condensation displays a high temperature spectrum with strong emissions of He II, N III], N IV], N V, Si III], Si IV, Fe III, and of the fluorescence Fe II 1785−88 Å lines. C II 1335 Å is also weakly present, while C III] 1907 Å and C IV 1550 Å are absent. An *interstellar* extinction of $E_{B-V}\simeq$0.4 is derived from the 2200 Å i.s. band in the nebular spectra.

Key words: line: profiles — circumstellar matter — stars: emission-line — stars: individual (η Car) — stars: mass loss — ultraviolet: stars

1. Introduction

This work is the continuation of the study performed by Viotti et al. (1989, hereafter Paper I) on the high resolution ultraviolet spectrum of the peculiar variable η Car. The star is known for the deep luminosity fading of the 19th century (e.g. Polcaro & Viotti 1993), the very high luminosity (about 5 10^6 $L_\odot$) and mass loss rate ($\sim$0.075 $M_\odot$ y^{-1}, Andriesse et al. 1978), and the very rich emission line spectrum in all the wavelength ranges. η Car is surrounded by a nebula elongated in the NW-SE direction which is also called the *Homunculus*.

Gaviola (1950) identified in the nebula many features, or condensations, which, according to the proper motion measurements of Ringuelet (1958), Walborn et al. (1978), van Genderen & Thé (1984), and Walborn & Blanco (1988) have been ejected during the paroxysmal phases of the 19th century. Thackeray (1956) found that the light from different parts of the Homunculus is strongly polarized in the direction perpendicular to the radius vector from the stellar core, which indicates that the radiation from the nebula is mostly scattered starlight. Further spectropolarimetric observations by Thackeray himself of the NW part of the Homunculus, the H condensation, have separated the unpolarized sharp low velocity spectral lines ([N II], [S II], [Fe II]) formed in the nebula, from the strongly polarized continuum and broad high velocity H I, He I and Fe II emission lines (Thackeray 1961). These

* Based on IUE observations obtained at the Villafranca Satellite Tracking Station of the European Space Agency, and on archive data collected from the Ultraviolet Low Dispersion Archive (ULDA)

observations allowed the determination of the expansion velocity of H condensation of 630 km s^{-1}.

High resolution infrared maps of the Homunculus were presented by Allen (1989). Both scattering in the nebula and 400 K thermal emission by dust were detected at 1.2–2.2 and 3.8–4.8 μm, respectively. It was deduced that the nebula is optically thin except very close to the star, and that the dust distribution can be described by a hollow, clumpy bipolar outflow. More recently, detailed studies have been carried out on the optical spatial structure of the Homunculus. Burgarella & Paresce (1991) identified some 40 knots in a field 21″×33″ around η Car, with an overall shape similar to that of bipolar nebulae. Observations in [N II] 6584 Å and V filters show a nitrogen overabundance in the nebula. Hester et al. (1991) performed high spatial resolution observations of the Homunculus with the HST Wide Field/Planetary Camera. An extension to the northeast of the star resembles a stellar jet, with its associated bow shock. The HST data indicate that the material around the star may be represented by an oblate shell, with polar blowouts, rather than a bipolar flow.

Hillier & Allen (1992) obtained many optical spectral maps of the Homunculus at resolution of 0.7 to 3 Å. They showed that the spectrum of the nebula arises from a combination of low-excitation intrinsic emission and from scattering of radiation originating in the central star. They derived a model for the Homunculus in which the SE lobe is an incomplete hollow shell expanding toward us, while the spectra of the NW region display two or more components on most emission lines. The NW region of the expanding shell is similar to the SE region, but is expanding away from us. Moreover, Hillier & Allen found significant profile variations in the central 3.6″×3.6″. In the Homunculus the equivalent widths of the H I and He I lines are 30% smaller than in the core, while those of [Fe II] are at least a factor 5 smaller.

The ultraviolet spectrum of the η Car nebula was reported in the earlier works of Viotti et al. (1981) and Davidson et al. (1982), who pointed out the anomalous strength of the nitrogen and He II lines in the X-ray emitting S condensation. More recently, Davidson et al. (1986) discussed the ultraviolet and visual spectroscopy of the shock–heated S condensation and of other regions around η Car, and found a helium abundance of roughly $Y \approx 0.4$, and that most of CNO is nitrogen.

In Paper I we discussed the high resolution ultraviolet spectrum of the η Car stellar core, and give the line intensity and identification. In this paper we discuss in detail the low and high resolution IUE observations obtained in December 1980, which were preliminarily presented by Viotti et al. (1981) and Viotti et al. (1986). The high resolution LWR spectrum of H condensation (the *head* of the Homunculus) is presented in the form of an Atlas and compared with that of the stellar core given in Paper I. We also analyze the low resolution IUE spectra of two bright regions of the Homunculus, and of the X-ray emitting S condensation.

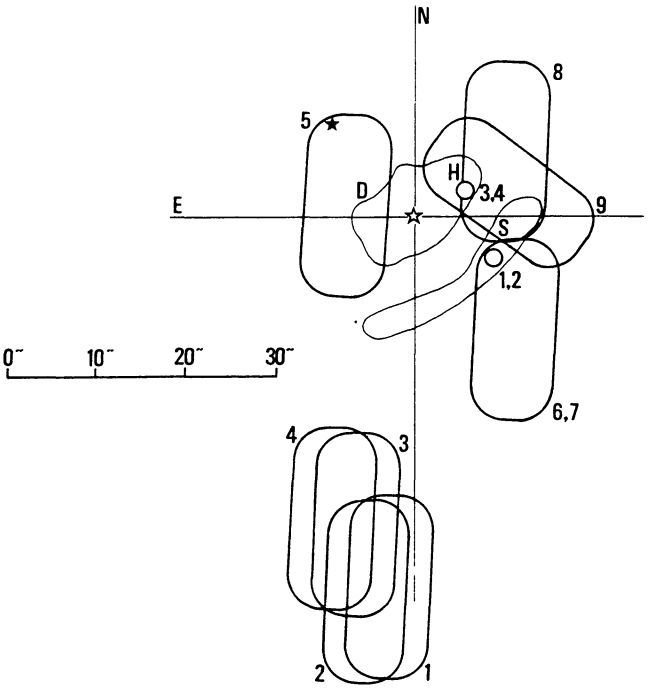

Fig. 1. Schematic map of the η Car region with the main nebular features. The approximate position of the IUE small circular (SA) and large 10″×20″ (LA) apertures is indicated. The position of η Car and of the star #64 near D is also marked. Each aperture is labeled as in Table 1. The LA position angles are 178° and 55° for the December 1980 and August 1981 images, respectively

2. Observations and data analysis

For this work we have used the spectroscopic material collected by us in the SWP (1200 to 1950 Å) and LWR (2000 to 3200 Å) modes during the December 1980 IUE observing run. The nebula of η Car was observed at low resolution near condensations H (the *head*), D (Homunculus' right leg), and S (the *shell*), and at high resolution in the LWR mode near H. The position of the centre of the IUE small and large apertures (SA and LA, respectively) is reported in Table 1 and illustrated in Fig. 1. These positions were derived from the x, y values of the aperture centres as reported in the IUE Observatory Log, and should be accurate to $\leq 1''$. The 1980 IUE observations of the nebula were compared with those of the central star obtained in 1978–1980. Actually, some care should be taken in this comparison since η Car is known to undergo shell episodes on a 5 yr time scale (Damineli Neto et al. 1994). But in our case the comparison is justified by the fact that during the considered period of time the star was nearly steady

Table 1. Log of the IUE observations of the η Car nebula

No.	IUE image	object	x y	$\Delta\alpha$ $\Delta\delta$	date	UT start	exp.	ECC	figure
	(1)	(2)	(3)	(4)		(5)	(6)	(7)	
1	L 3 10759 SA	S	−05 +41	5″S 9″W	05 Dec 80	10:45	1200	121	4d
2	L 2 09440 SA	S	−05 +41	5″S 9″W	05 Dec 80	11:09	1200	231	4d
3	L 3 10760 SA	H	+17 +18	3″N 7″W	05 Dec 80	11:55	3600	202	4b
4	L 2 09441 SA	H	+17 +17	3″N 7″W	05 Dec 80	13:06	1800	102?	4b
5	L 2 09442 LA	D	−06 −28	1″N 8″E	05 Dec 80	16:51	2580	702	4f,5
6	L 2 09452 LA	S	−32 +59	13″S 12″W	07 Dec 80	15:06	2400	572	4e
7	L 3 10778 LA	S	−32 +59	13″S 12″W	07 Dec 80	15:51	3000	232	4e,6
8	H 2 09453 LA	H	+37 +29	8″N 10″W	07 Dec 80	16:54	3240	472	2,3,4c
9	H 3 14571 LA	H	−40 +24	3″N 12″W	13 Aug 81	23:59	4680	101	=

Notes to the table: (1) IUE image number. H: high resolution, L: low resolution, 1: LWP, 2: LWR, 3: SWP, SA: small aperture, LA: large aperture. (2) Object name (Walborn 1976). (3) Displacement of the aperture centre with respect to the central star in the IUE focal plane. (4) Displacement in right ascension and declination (see Fig. 1). (5) UT of exposure start (hours and minutes). (6) Exposure time (sec). (7) IUE exposure code for continuum, emission lines and background.

Notes on individual images: SWP10759 and LWR9440: during the SA exposure the LA was left open at about 42″ from η Car (see Fig. 1), with no signal. SWP10760: the LA was left open at about 30″S of η Car. LWR9441: same position as SWP10760. LWR9442: the LA includes condensations C and D, and, marginally, the star #64 of the Feinstein et al. (1973) catalogue. The spectrum is saturated longward of 2420 Å. LWR9452 and SWP10778: the large aperture is shifted to SW with respect to the position of the condensation S, which is near its edge, in order to minimize the scattered light from the central star. LWR9453: the large aperture is shifted to NW with respect to the position of H condensation in order to minimize the scattered star light. SWP14751: the large aperture partly includes the feature S. No detectable spectrum.

(see also Whitelock et al. 1994). On the contrary, the IUE images obtained in the following period July-August 1981 cannot be used for comparison as the star at that time underwent a new shell phase (Zanella et al. 1984).

The high resolution spectrum of H condensation has been studied using the IUE "extended line–by–line" file of the reprocessed LWR9453 image (#8). In order to minimize the instrumentally scattered starlight, or *stray light* which could strongly affect the observations (e.g. Hillier & Allen 1992), the IUE aperture has been located in order to include only the Homunculus head, far enough from the stellar core. The effect of the stray light in the IUE images has been studied in detail by de Boer & Cassatella (1986) and by Cassatella (1986). Witt et al. (1982) and Viotti et al. (1988) discussed the problem in their IUE study of the nebulae surrounding the early type stars HD 200775 and AG Car. According to de Boer & Cassatella (1986) the surface density (per sterad) $S_{\rm stray}(r)$ of stray light relative to the stellar flux F_*, at a distance $r \leq 40''$ from the central star is given, in the 2000–3200 Å range, by: $\log S_{\rm stray}(r)/F_* = 9.46 - 3.35 \log r$. Hence, for the image #8 the stray light is maximum near the eastern edge of the LA, and rapidly decreases towards west along the minor axis of the IUE large aperture. We have integrated the stray light over the IUE aperture using the above formula, and taking into account the instrumental vignetting near the LA border as for instance described in Fig. 5 of Viotti et al. (1988). The resulting stray light flux in the image #8 turns out to be $F_{\rm stray} = 3–6\ 10^{-3}\ F_{\rm star}$, with a weighted mean distance from the stellar core of 8–9″.

The nebular emission should mostly originate from the region of the LA which overlaps the NW *head* of the Homunculus (about 6″–7″ from the stellar core), where also the stray light is maximum. (Note that, as discussed below, the line profiles do in fact suggest that the observed spectrum is actually coming from a narrow region). The comparison of the star's and nebular atlases gives $F_{\rm obs}/F_{\rm star} \simeq 0.14$, which implies $F_{\rm obs}/F_{\rm stray} = 25–50$, where the range is related to the uncertainty in the effective area giving rise to the target's emission, and in the IUE aperture position. We therefore conclude that for the image #8 the amount of instrumentally scattered light is negligible.

The IUE data were converted into absolute fluxes using standard calibration and ripple correction methods, and the resulting fluxes (in 10^{-14} erg cm^{-2} s^{-1} for a 10″×20″ sky area) have been used for the Atlas in Fig. 2. The Atlas consists of plots covering 55 Å each, including 5 Å wavelength overlapping between adjacent regions, and covers the range from 2295 Å to 3200 Å. The same spectral intervals of Paper I (Viotti et al. 1989, from page 990 to page 994) were used, so that comparison can be made between the core and the nebular spectrum. Some interesting spectral regions of the nebula, which will be discussed in Sect. 4, are shown in Figs. 3a, b and compared with those of the stellar core. No measurable signal

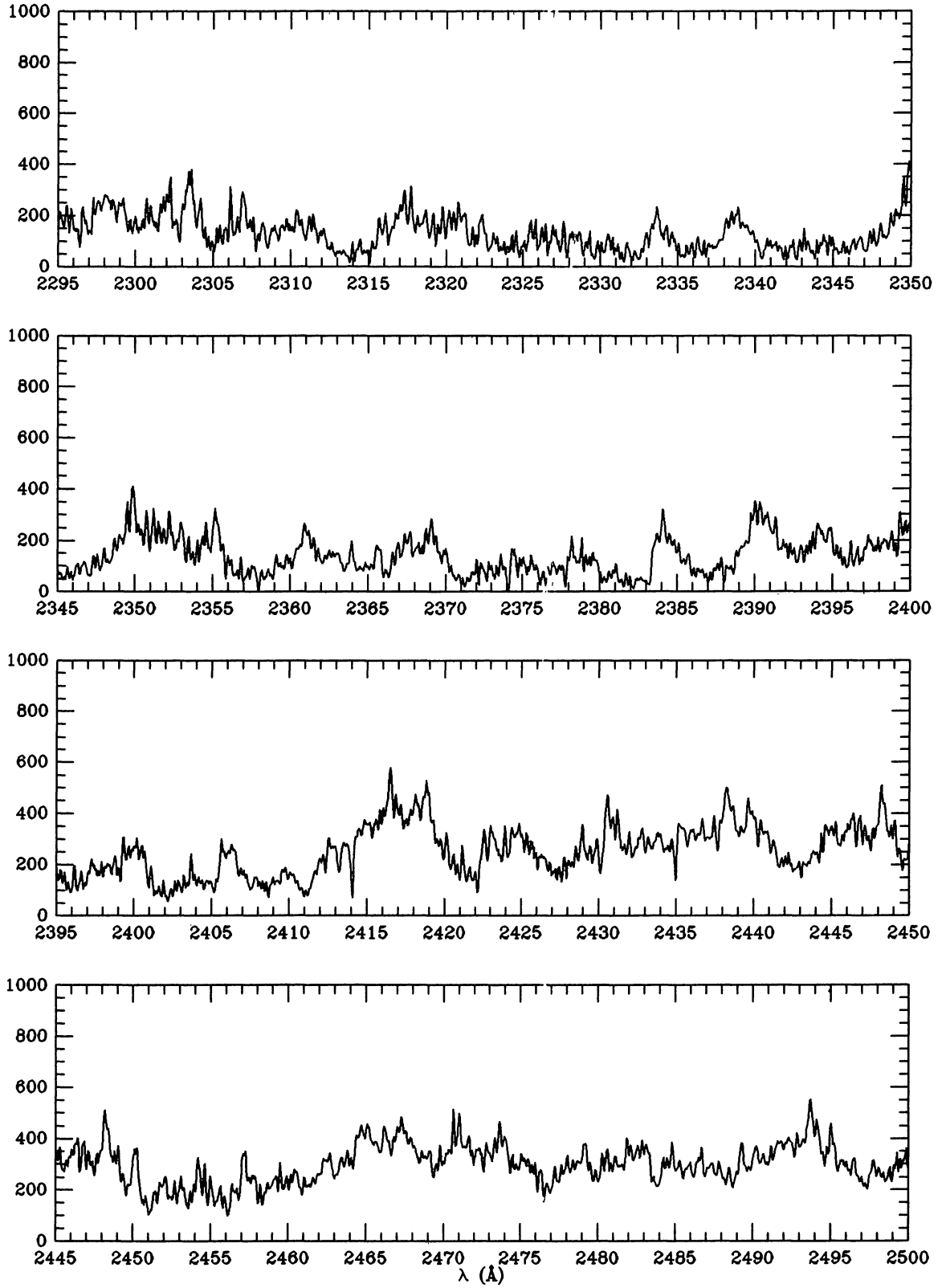

Fig. 2. Atlas of the high resolution ultraviolet spectrum (LWR9453, 2295–3200 Å) near the η Car H condensation. Ordinates are 10^{-14} erg cm^{-2} s^{-1}Å^{-1} in a $10''\times20''$ projected area. The strongest features are shown in Fig. 3. Reseau marks and gaps between adjacent echelle orders are indicated with an asterisk (*)

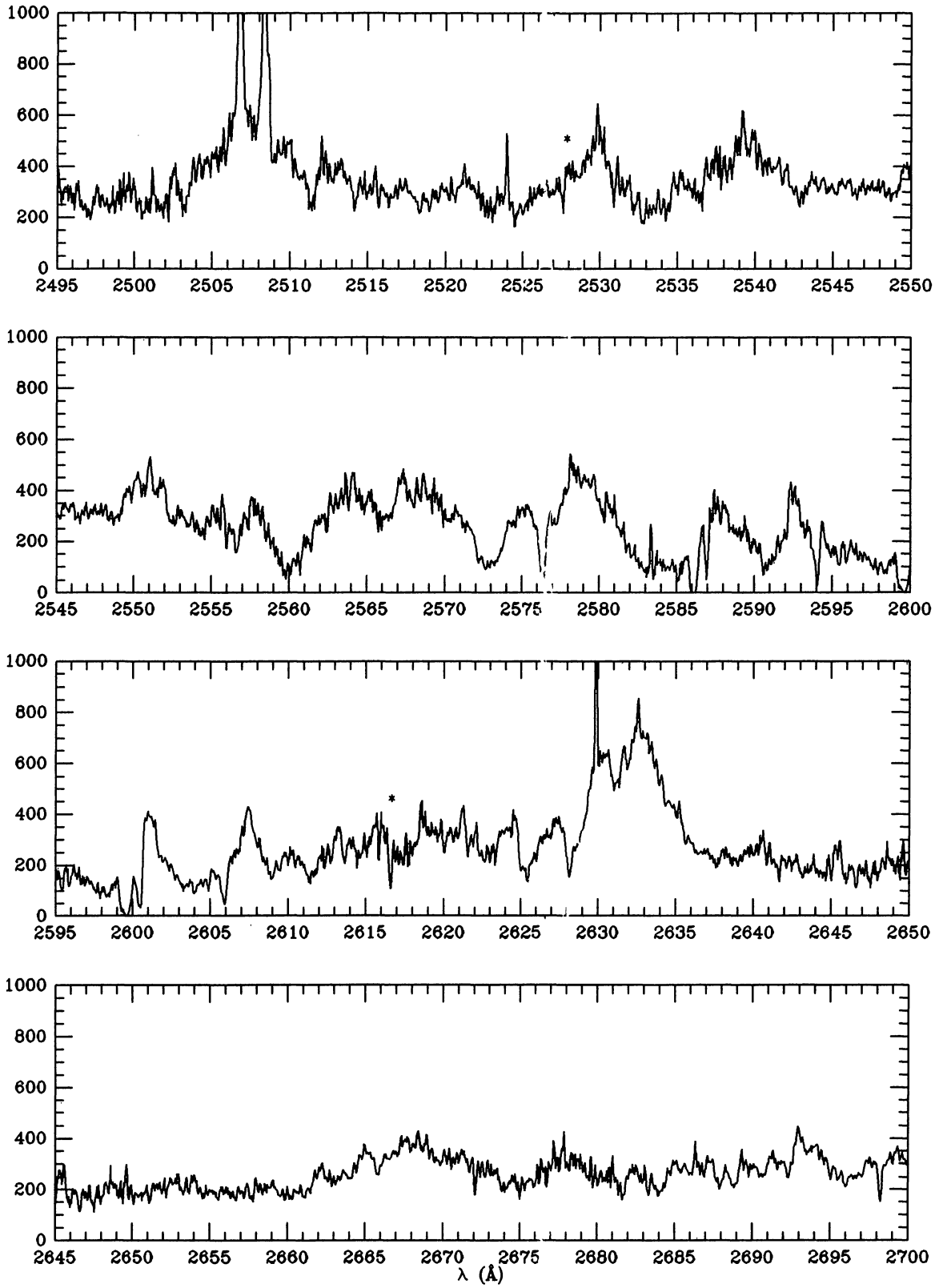

Fig. 2. continued

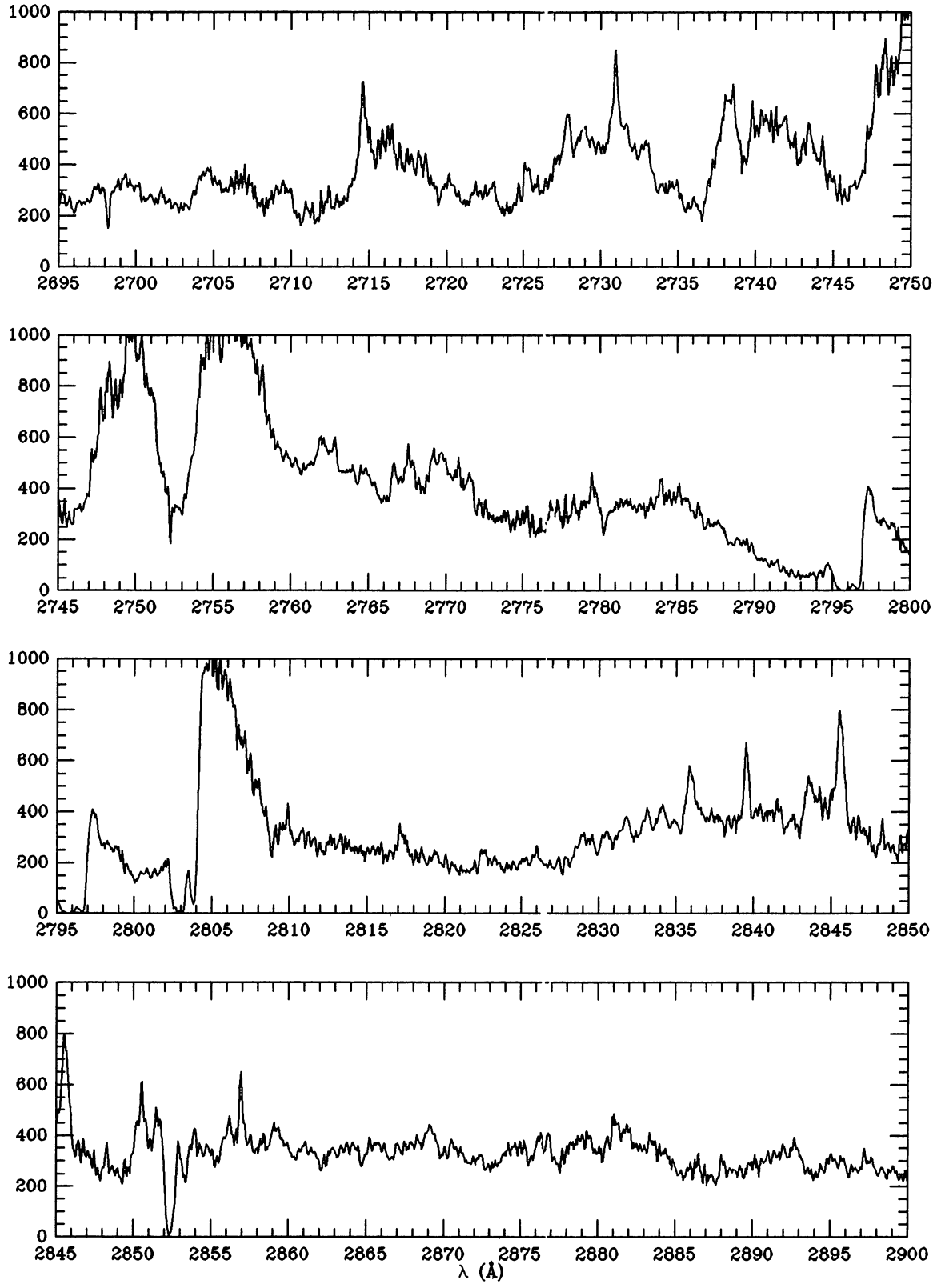

Fig. 2. continued

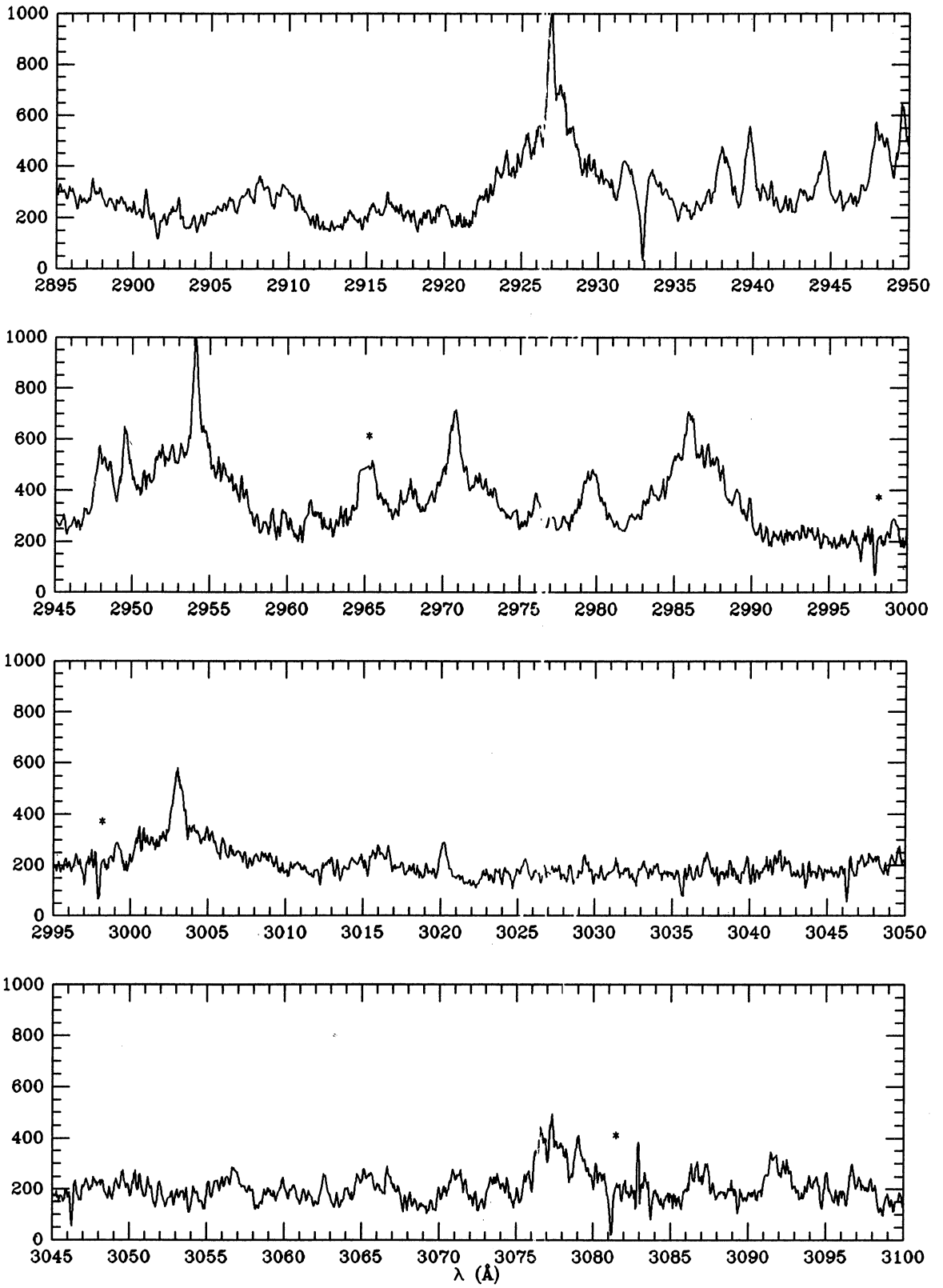

Fig. 2. continued

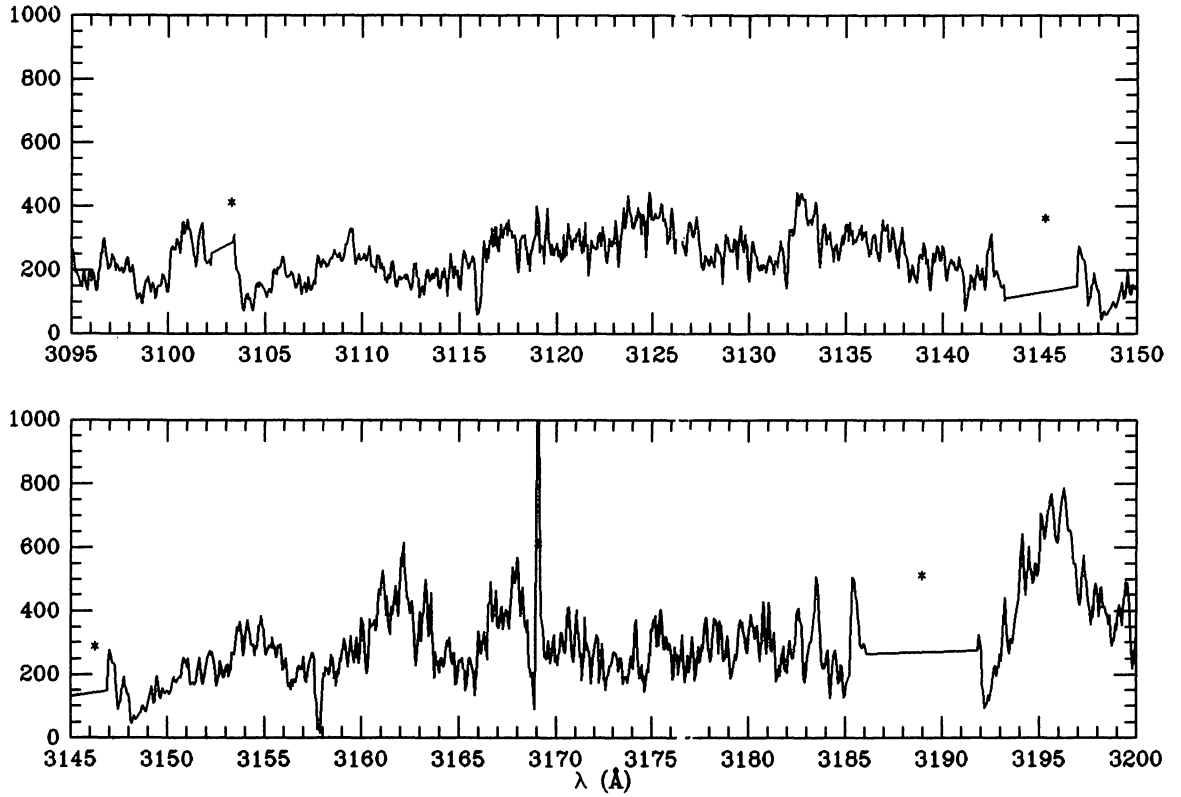

Fig. 2. continued

is present in the high resolution SWP14571 image of the same region obtained in August 1981.

The high resolution spectrogram given in Fig. 2 of the Atlas was measured following the procedure described in Paper I, and the results are reported in Table 2 where the successive columns give: (1) Observed barycentric wavelength. (2) Type of the line: absorption (A) or emission (E). (3) Total width of the measured feature (in Å). (4) Line equivalent width (in Å); ":" = uncertain measurement. (5) Adopted continuum level in 10^{-14} erg cm^{-2} s^{-1} Å^{-1} local to the feature, not corrected for the interstellar absorption. (6) Identification of the ion contributing to the observed line. (7) Laboratory wavelength. (8) Remarks: "PCyg" = P Cygni violet-shifted absorption; "i.s." = interstellar line; "bl" = blended with the nearby line; "broad em" = broad emission line; "em peak" = narrow emission peak, sometimes part of a broad emission line; "fl" = line excited by fluorescence; "db" = double line; possible contributors are also indicated. An asterisk (*) indicates a comment in the notes of the table. Since the IUE target is not a point source, but a diffuse emission not uniformly filling the IUE aperture, a systematic error in the wavelength scale could be present. We have in fact found that the mean radial velocity of the main component of the interstellar lines is +43±2 km s^{-1}, while the correct value is close to zero. This positive shift clearly suggests that the emission is mostly coming from a narrow region slightly shifted towards south with respect to the LA centre, in good agreement with the position of the Homunculus' *head* in the IUE large aperture (Fig. 1). The narrowness of the emitting region is also confirmed by the profile of the interstellar lines in the Atlas, which is only slightly larger than in the stellar core (see also Fig. 3c below). In the following discussion all the measured radial velocities have been corrected by −43 km s^{-1} in order to have, like in Paper I, the velocity scale referred to that of the main interstellar line system. (Note however that in the Atlas in Fig. 2 the original wavelength scale has been used).

As for the low resolution spectra we have used the one-dimensional extracted spectrograms of the ULDA database for both the SA and LA images. It must be noted that ULDA also includes the LA spectra of the images #1 to #4 in Table 1, which however are referred to a region very far from η Car, as illustrated in Fig. 1. Indeed, these LA spectra appear very weak or featureless. The stray light is negligible in all the images with the possible exception of the central spectral strips of the image #5, as discussed below.

The spectra of the different parts of the η Car nebula as well as of the stellar core are reported in Fig. 4. The nebular spectra in the figure have been slightly smoothed, and the geocoronal Lyα emission cut off. For the stellar core we used the small aperture spectrum of SWP1600

Table 3. The low resolution ultraviolet spectrum of the condensations of η Car in December 1980

	H COND SA SWP10760S+LWR9441S				S COND SA SWP10759S+LWR9440S				S COND LA SWP10778L+LWR9452L			
LAB WL	OBS	CONT	WID	FLU	OBS	CONT	WID	FLU	OBS	CONT	WID	FLU
(1)	(2)	(3)	(4)	(5)	(2)	(3)	(4)	(5)	(2)	(3)	(4)	(5)
1240	44.5?	0.53	18	31:					31.7	4.4	30	130
1304	06.1	1.1	28	37:					05.9	3.3	23	77
1400	94.1	1.6	29	36::					92.0	6.4	25	87
1486	83.9?	2.4	14	21::		p?			81.7	7.5	35	120
1530	29.3	2.1	13	35:		p?			26.3	7.5	19	472
1641		p?				p?			33.9	6.0	18	51
1750	45.8	2.3	25	50	44.5	0.49	16	38::	44.7	5.5	36	314
1786	84.2	2.3	25	37					81.3	6.0	23	46
1812	07.5	2.3	28	40					10.1	5.5	24	61
1890	91.8	2.7	23	19		p?			81.9	5.8	26	84
1915	13.2	2.4	19	14:					07.1	5.0	21	26
2630	19.4	3.3	61	298					19.8	5.6	62	465
2750	51.3	4.4	45	281					52.0	9.6	64	329
2800	03.1	5.2	33	270	97.4	0.98	25	74	00.4	9.7	32	568

Notes to the table: (1) *1240*: N V 1238.8, 1242.8. *1304*: O I 1302.2–04.9–06.0, Si II 1309.3. *1400*: Si IV 1393.8–1402.8. *1486*: N IV 1483.3–86.5. *1530*: Si II 1526.7–33.4. *1641*: He II 1640.6. *1750*: N III] 1748.3–49.7–52.2–54.0. *1786*: Fe II 1785.3–86.7–88.0. *1812*: Si II 1808.0–16.9. *1890*: Si III] 1882.7–92.0. *1915*: Fe III 1914.9. *2630*: Fe II 2611.9–17.6–25.7–31.2. *2750*: Fe II 2724.9–27.5–30.7. *2800*: Mg II 2795.5–2802.7. (2) Observed barycentric wavelength (in Å). (3) Continuum level local to the feature (in 10^{-14} erg cm^{-2} s^{-1} Å^{-1}). (4) Total width of the measured feature (in Å). (5) Emission line flux (in 10^{-14} erg cm^{-2} s^{-1}).

obtained on May 22, 1978 (the LA spectrum is overexposed), and the LA spectrum of LWR4258 obtained on April 13, 1979. The SWP fluxes have been multiplied by a factor 2 in order to take in some account the different aperture size.

The measurements of the most prominent lines are reported in Table 3, which gives the line barycentre, the width of the measured feature, the continuum local to the feature (in 10^{-14} erg cm^{-2} s^{-1} Å^{-1}), and the line flux (in 10^{-14} erg cm^{-2} s^{-1}).

The LA images of the nebula (#5 centered on D condensation, and #6 and #7 centred on S condensation) can be used for the analysis of the spatial distribution of the UV radiation in the direction along the major axis of the aperture. To this purpose we have analyzed the two-dimensional line-by-line IUE third file in which the LA images are sampled at $\sqrt{2}/2$ pixels (corresponding to 1.″078 on the sky, cf. Viotti et al. 1988) perpendicular to the dispersion, so that the full aperture is scanned by about 20 samples. Therefore, for each sample the integrated flux from a projected sky area of about 10.8″^{2} is measured.

3. The ultraviolet spectrum of the nebula

3.1. *The LWR high resolution spectrum of H condensation*

As for the long wavelength spectrum of the H condensation (LWR 9453) the large aperture collects photons from nebular regions from ∼6″ to ∼17″ from the stellar core, but, as discussed above, the bulk of the emission comes from the bright H condensation. The high resolution spectrum includes many features hard to identify because of line blending and large noise especially at the shortest wavelengths. The line identification in Table 2 was essentially based on that of the η Car stellar core given in Paper I. Most features belong to atomic transitions of singly ionized metals, mainly Fe II.

The resonance and lower excitation lines present an extended P Cygni profile (Figs. 3b and 3c).

The absorption component has a barycentric radial velocity (referred to the interstellar velocity) ranging from −190 to −320 km s^{-1}, depending on the line strength (larger violet shift for stronger lines), and an edge velocity of −400 to −550 km s^{-1} (excluding the Mg II resonance doublet which will be discussed below). However, this could be considered as a lower limit because the noise and the severe line blending do not allow a precise

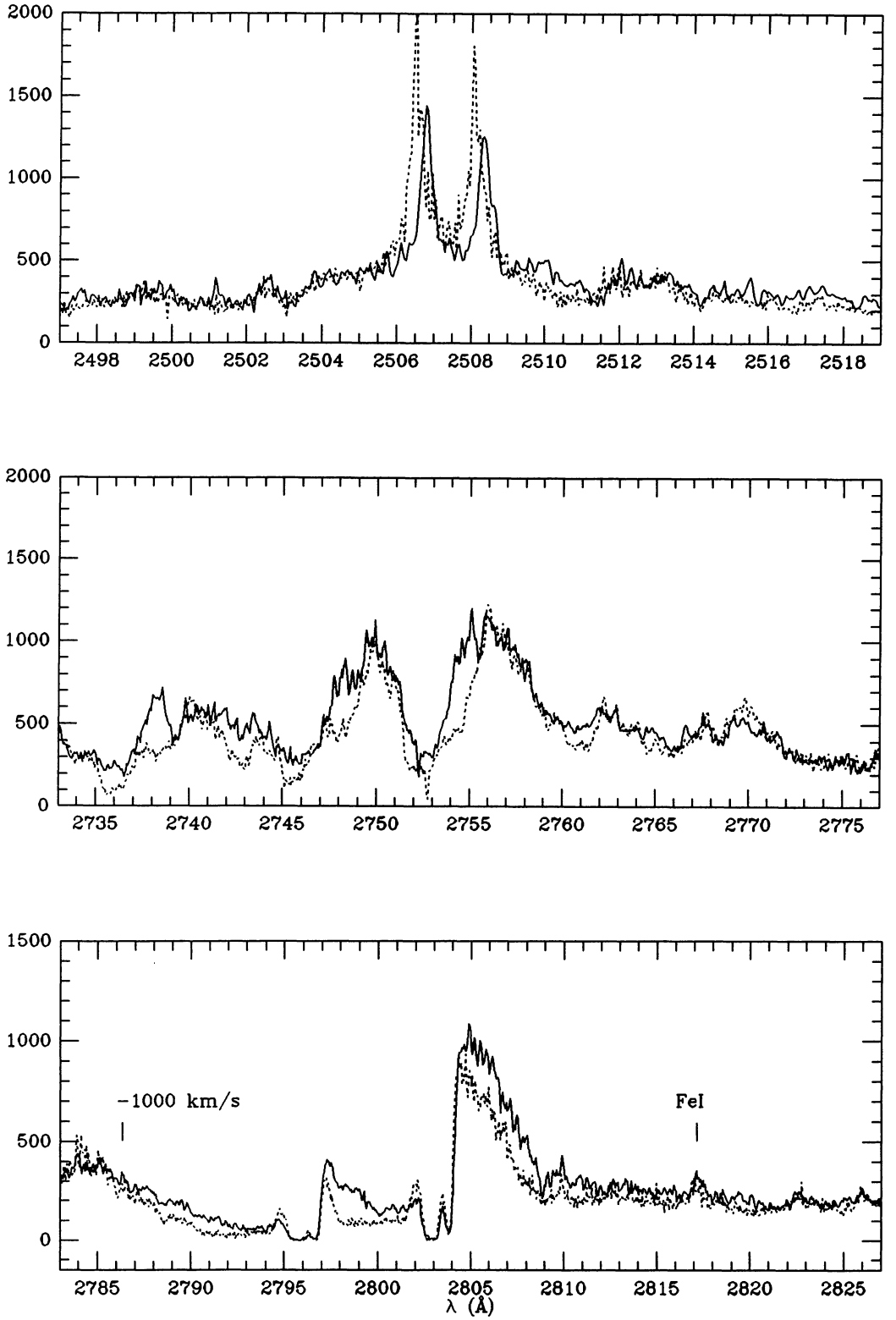

Fig. 3. Comparison of the high resolution ultraviolet spectrum of H condensation in December 1980 (continuous curve) with that of the stellar core in April 1979 (dotted curve). Nebular fluxes are the same as in Fig. 2. The stellar core fluxes have been reduced by a factor 7 in order to overlap with the nebular spectrum. The stellar core spectrum LWR 1592 is saturated near 2506−8 Å and 2804 Å, and has been replaced with the less exposed LWR 3890 spectrum

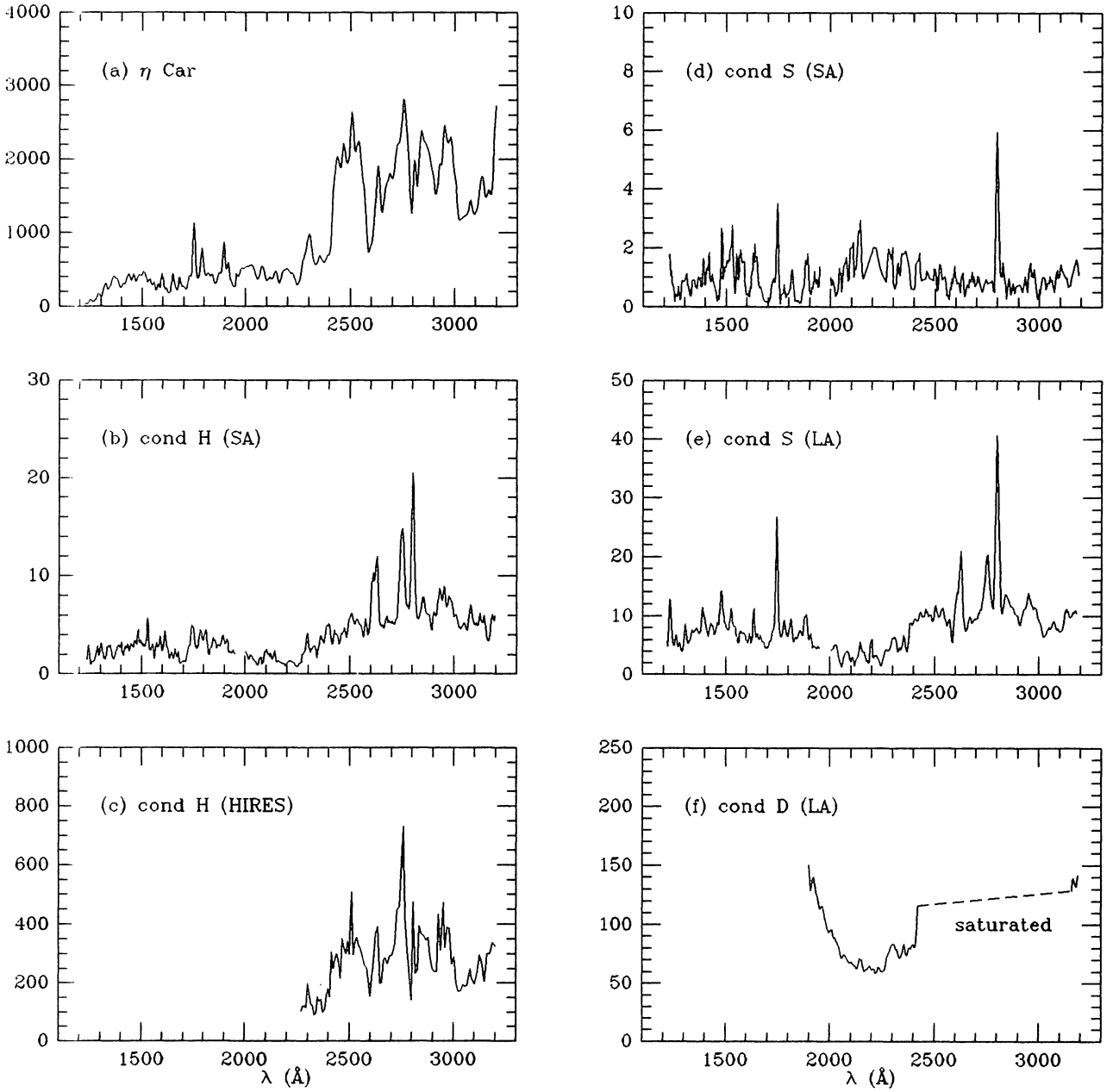

Fig. 4. The low resolution IUE spectrum of η Car, and the nebular condensations. a) η Car in 1978-79, IUE images SWP1600S (multiplied by a factor 2) and LWR4258L. b) H condensation, SWP10760S + LWR9441S. c) H condensation, LWR 9453 smoothed high resolution. d) S condensation, SWP10759S + LWR9440S. e) S condensation, SWP10778L + LWR9452L. f) D condensation, LWR9442L. The strongest emission lines are indicated

measure of the blue line wings. The emission components have a barycentric velocity of +50 to +120 km s^{-1}. In general they display a main emission peak at +15 km s^{-1}, which is much smaller than the radial velocity reported by Hiller & Allen (1992) in their optical study of the NW lobe of the Homunculus. In a few cases, however, a second peak at +170 km s^{-1} is present, which is consistent with one of the components at 5″NW observed by Hillier & Allen (1992, Fig. 15). We have compared the Fe II line profiles from the December 1980 spectrum of H condensation with those of the stellar core from Paper I. As shown in Fig. 3, the P Cygni profiles appear similar, but the absorption components are deeper in the stellar spectrum and have much larger equivalent widths, whereas the broad emission components are generally more diffuse and more intense in the nebular spectrum. Clearly, the spectrum partly arises from dust scattering of the radiation of the stellar core. The scattering should in fact produce the observed

broadening of the emission features and a partial filling-in of the P Cygni absorption. The smaller redshift of the emission components with respect to the optical observations of Hillier & Allen (1992) can be accounted for at least partly by the more extended region of the nebula sampled by the IUE large aperture. In addition, the larger continuum and line opacity in the UV could mask the radiation originating from the opposite side of the Homunculus, which has a projected velocity more negative than that of the core of the H condensation. This should produce a line redshift smaller than in the optical.

The Mg II doublet is the most interesting feature in the UV nebular spectrum (Fig. 3). The Mg II *h* component is characterized by a prominent red emission which peaks at 2805 Å, and by a red wing extending to about 2809−2810 Å. The blue side of the emission is largely depressed by the two interstellar lines and by the strong P Cygni absorption component. In addition, the Mg II *h* absorption features almost totally absorb the red wing of the Mg II *k* emission, leaving out only a weak narrow emission dip at 2797.5 Å, corresponding to about −600 km s^{-1}, which could be considered as an upper limit of the absorption edge velocity. The shorter wavelength side of the Mg II *k* line profile is dominated by the double interstellar feature and by the extended P Cygni absorption. It should be noted that the minimum depth of the Mg II *k* feature is lower than that of the corresponding Mg II *h* P Cygni absorption line. This has to be attributed to the presence of a strong residual absorption of the Mg II *h* P Cygni line, which therefore extends to at least about 2792 Å, corresponding to a limiting velocity of ≤ -1000 km s^{-1}. Concerning the absorption of the Mg II *k* line, it can be evaluated from the wavelength at which its short-wavelength wing reaches the continuum level. Assuming for the latter a value of about 3 10^{-12} erg cm^{-2} s^{-1} $Å^{-1}$ as estimated from the nearby line free regions, we find a wavelength limit for the Mg II *k* line of about 2786.4 Å, i.e. a radial velocity limit of about −1000 km s^{-1}. But the absorption could extend to even shorter wavelengths. The slight flux excess at 2784−85 Å with respect to this continuum level could be attributed to the presence of unresolved high excitation emission lines of Fe II λ2783.69 and λ2785.21 (see Paper I). The above considerations can also be applied to the profile of the Mg II doublet in the stellar spectrum. As seen in Fig. 3b the two profiles are rather similar, but for deeper P Cygni absorptions in the stellar spectrum with a nearly zero minimum flux, which seems again to be in agreement with the hypothesis that at least part of the lines are originated from starlight scattered by the nebular dust.

The UV spectrum of H condensation also shows many narrower emission lines identified as high excitation Fe II transitions, which clearly are nebular in origin. Of particular interest are the fluorescent lines at 2506.80 Å and 2508.34 Å, which in the nebular spectrum are characterized by two narrow peaks at 2507.0 Å and 2508.5 Å (Fig. 3a). These lines are redshifted by +55 km s^{-1} with respect to the stellar ones (the interstellar spectrum being the wavelength reference frame for both). The lines are superimposed over a shallow broad emission which is also seen in the stellar spectrum. In both cases the broad component is more extended towards shorter wavelengths. Note that a weak unidentified emission at 2504.81 Å has been observed in the ultraviolet spectrum of the symbiotic star RR Tel (Penston et al. 1983): this line might contribute to the blue wing of the emission, and at least partly explains its asymmetry.

We have identified two weak emission lines at 2823.0 and 2844.0 Å with the fluorescently excited Fe I emission lines at 2823.28 and 2843.98 Å (the latter probably blended with Fe II 2843.32 and 2843.49). Since in Paper I we have not found an emission at 2823 Å in the spectrum of the stellar core, we have reanalyzed that spectrum and compared with the nebular one. As shown in Fig. 3c an emission feature is clearly present in both spectra at the right position, and this, together with the presence of the other emission at 2844 Å, gives more strength to our identification. Indeed, these two lines are expected to be the most prominent features of neutral iron in a stellar chromosphere for being fluorescently excited by the very intense Mg II *k*-line ambient emission (e.g. Carpenter et al. 1988). The fluorescent Fe I λ2823.28 line has been also identified in the Fe II rich UV spectrum of KQ Pup (Altamore et al. 1981). Fe I emission lines have been previously identified by Gaviola (1953) in the optical spectrum of η Car, but a later more accurate analysis of the same material has shown that all the identified lines belong to transitions of other ions (Viotti 1968). Fe I violet shifted absorptions were observed in the 1893 spectrum of η Car during its 1887−1895 light maximum (Whitney 1952). The present one can therefore be considered as the first identification of Fe I in the spectrum of η Car during its present minimum phase.

It should be finally noted that many interstellar lines are present in the nebular spectrum which have the same strength (within the errors) of those observed in the stellar spectrum discussed in Paper I. The main components appear slightly broad and marginally double, like in the core spectrum. In addition many interstellar lines display a red component at +94 km s^{-1}, very close to the +100 km s^{-1} component of the core spectrum, which is associated with the high velocity 'violent' medium in the Carina nebula.

3.2. *The low resolution spectrum of the nebula*

Figure 4 shows the low resolution ultraviolet spectrum of η Car and of the different regions of the Homunculus indicated in Fig. 1. H condensation (Fig. 4b) has been observed with the IUE small aperture (SA) centred near the *head* of the nebula (about 8″NW of η Car). Its UV

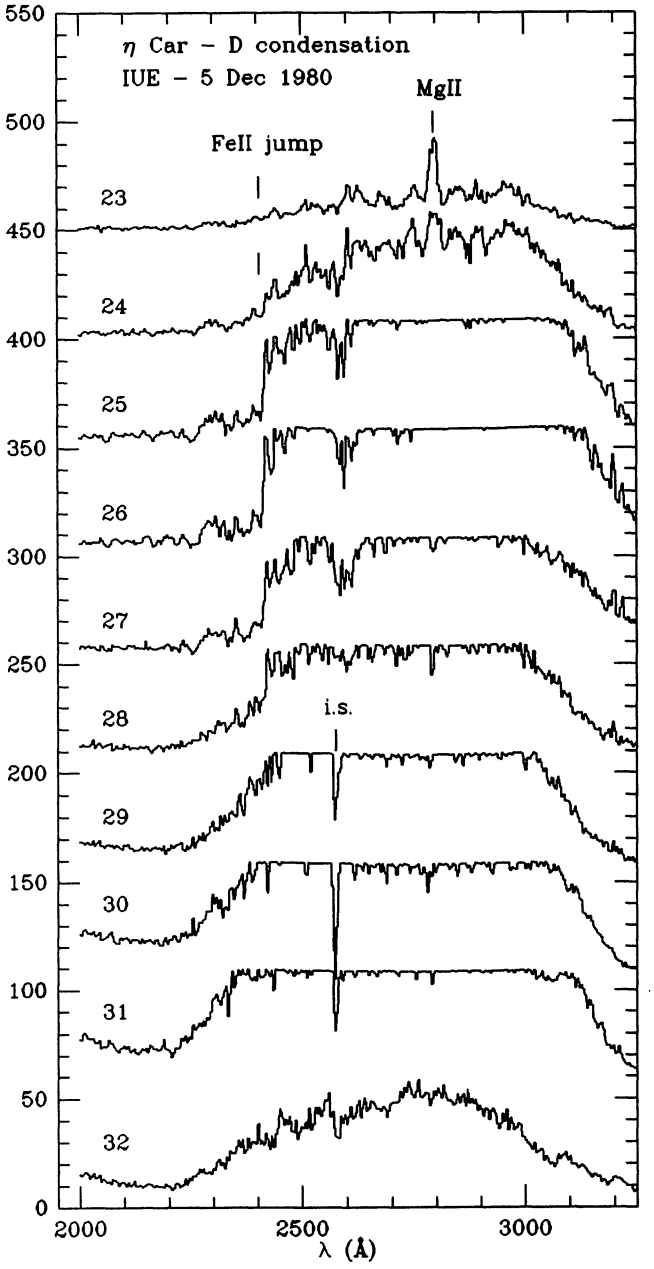

Fig. 5. Spatially resolved spectral map of D condensation (IUE image LWR9442L, #5 in Fig. 1). From top to bottom: spectral orders 23 (South) to 32 (North). Individual orders are vertically shifted each others by 50. Ordinates are fluxes in 10^{-11} erg cm^{-2} s^{-1} per 10.8″^{2}. Note the 2400 Å *Fe* II *jump* in the spectra 25 to 28, which indicates that the central orders are mostly scattered light from the central star. These orders could be affected by the instrumental stray light. The interstellar 2200 Å band is clearly visible in the higher order spectra. The interstellar line blend at 2600 Å (Fe II and Mn II) is also indicated. Order 32 probably is the spectrum of the star #64. Fe II and Mg II are very prominent in emission in the southern part of the image

spectrum is characterized by a reddened continuum and a few prominent emission blends of Fe II λ2630 and λ2730, and Mg II λ2800. The strength of these lines indicates the presence of a high density, low temperature emitting gas. The LWR range of this spectrum is substantially different from the high resolution one discussed in the previous section. This difference is probably due to the fact that, because of satellite pointing problems, the actual distance of the SA from the central star was at least 2″–3″ larger than that shown in Fig. 1, while, as discussed above, the weighted mean distance of the high resolution LA image #8 is about 6″–7″. As for comparison, we show in Fig. 4c the spectrum #8 binned to the IUE low resolution. The high resolution spectrum appears intermediate between #4 and the stellar core, with a rather strong continuum with many absorption features, including the 2400 Å Fe II jump, which is less pronounced than in the stellar core spectrum (Fig. 4a). This discontinuity is due to the blending of very many Fe II absorptions near 2400 Å, and is a distinguishing feature of the spectrum of η Car (Paper I). The emission lines in the binned #8 spectrum are rather prominent, but much less than in #4. Conversely, the fluorescent Fe II λ2506–08 emission is much weaker in #4, in agreement with its formation in higher density regions.

The weak N III] λ1750 line could be originated in hotter regions outside the Homunculus. The continuum is depressed near 2200 Å by the interstellar band, whose strength corresponds, for a normal interstellar extinction law, to a colour excess of E_{B-V}=0.6±0.1.

The SA spectrum of S condensation (Fig. 4d) is very weak, and only the Mg II λ2800 and, possibly, N III] λ1750 lines can be identified. Many more lines are seen in the much better exposed LA spectrum of the same region (Fig. 4e), which however also includes other nearby regions. The most interesting feature of this latter spectrum is the presence of strong high temperature emission lines, such as N IV] 1483–86 Å, and He II 1641 Å, which, as already noted by Viotti et al. (1981) and Davidson et al. (1982), are much weaker or absent in the core spectrum. Also N V 1238-40 is strong in emission in the S shell, while in the star it is represented by a broad P Cygni absorption. Another peculiarity is the enhancement of the nitrogen lines with respect to the carbon ones, which led Davidson et al. (1986) to conclude that the matter ejected from η Car is nitrogen enriched. In our spectra, carbon is only represented by the C II 1335-6 Å resonance doublet (marked with 2 in Fig. 6), while silicon is present with three ionization stages. The continuum is quite structured for the presence of many unresolved absorption features at roughly the same position of those observed in the stellar core spectrum. The continuum energy distribution is however quite different with a much larger SWP/LWR flux ratio with respect to the stellar spectrum, which might be associated with the higher temperature of this X-ray emitting region. The difference can also be explained by

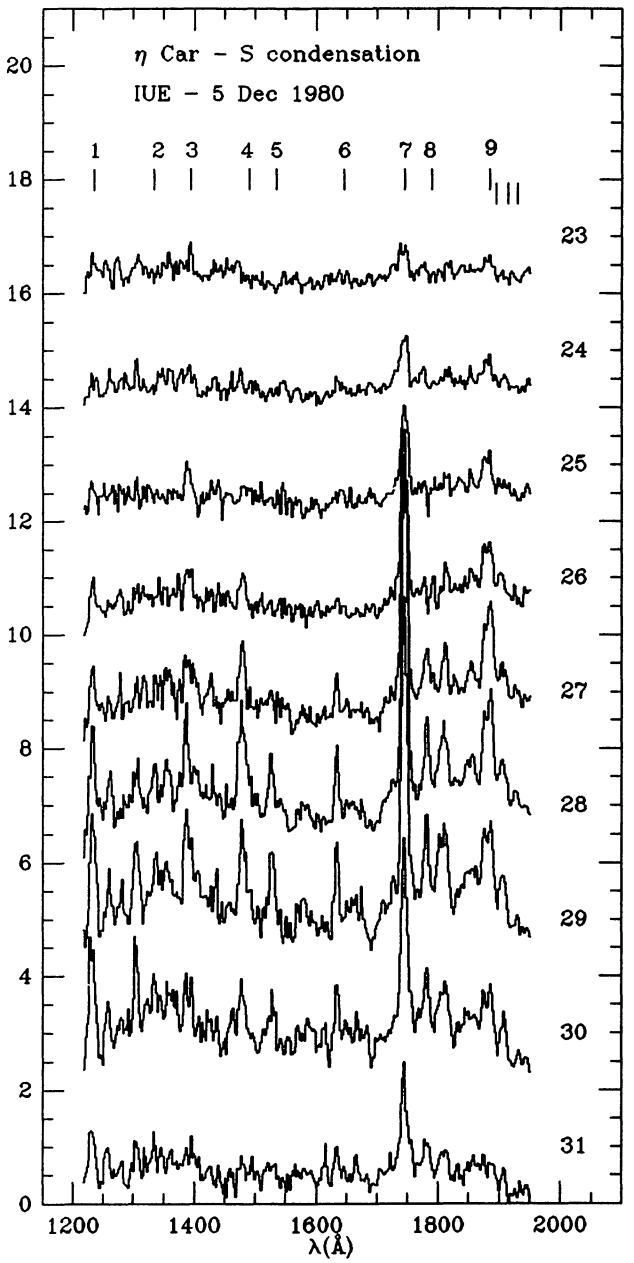

Fig. 6. Spatially resolved spectral map of S condensation (IUE image SWP10778L, #7 in Fig. 1). From top to bottom: spectral orders 23 (South) to 31 (North). Individual orders are vertically displaced each others by 2. Same ordinates as in Fig. 5. The geocoronal Lyα has been cut out of the spectrograms. Vertical bars are referred to the following lines: 1. N V 1239–43 Å, 2. C II 1335–6 Å, 3. Si IV 1394–1403 Å, 4. N IV] 1486 Å, 5. Si II 1527–33 Å, 6. He II 1641 Å, 7. N III] 1749–54 Å, 8. Fe II 1785–88 Å (multiplet 191 fluorescent lines), 9. Si III] 1892 Å. The last three bars are referred to the Fe III $\lambda\lambda$1895, 1915, 1926 triplet. The high temperature lines (He II, N V, N IV]) are particularly strong in the orders from 27 to 30. Note the absence of C IV 1550 Å

the additional circumstellar absorption affecting the radiation from the central star, as for example discussed by Andriesse et al. (1978).

The 2200 Å interstellar band is suggestive of a colour excess of E_{B-V} =0.4±0.1. The N III] λ1750 line is much stronger than in H condensation, indicating a higher ionization stage. Conversely, the long–wave spectra of the two regions are quite similar, with strong emission blends of Fe II 2600 and 2750 Å, and Mg II 2800 Å.

The eastern part of the Homunculus (D condensation) has been observed only in the LWR range with the large aperture, but most of the spectrum was saturated (Fig. 4f). Yet the interstellar 2200 Å band is clearly visible, and corresponds to E_{B-V} = 0.35±0.05. This image is discussed in detail below. All the above determinations of the interstellar extinction are in good agreement with the mean reddening of E_{B-V}=0.4–0.5 derived from the nearby stars, as for instance discussed by Feinstein et al. (1973), and confirm that this can be taken as an estimate of the true *interstellar* colour excess of η Car, while an additional *local* anomalous reddening of $E_{B-V}\simeq$0.7 arises from the immediate surroundings of the star (cf. Andriesse et al. 1978).

3.3. *The spatially resolved spectrum of the nebula*

Two parts of the homunculus have been pointed with the IUE large aperture (LA) in order to study the spectral variation throughout the nebula, which could tell us about its geometrical structure. A LWR image has been obtained in order to include the D condensation, 5″ East of the star (Fig. 1), i.e. the "right leg" of the homunculus. The central parts of the image are largely overexposed. Nevertheless, important information can the same be derived from the better exposed shorter wavelength regions, and from the image edges (the lower and higher spectral orders).

Figure 5 gives a plot of 11 uncalibrated spectral orders through the IUE image of D condensation; the lower orders are referred to the southern part of the image, towards the SE edge of the arc-shaped shell S. The spectrum of this region is essentially composed of prominent emission lines of Fe II and Mg II, and of a weak continuum with many absorptions of Fe II, and of a few strong interstellar lines, as well. The Mg II emission is saturated in #24. Note the similarity of these spectra with the SA spectra of H and S condensations shown in Fig. 4. In the following spectral orders, from #25 to #27, the unsaturated shortwave continuum is quite similar to the stellar one (Fig. 4a) with a strong 2400 Å *jump*. The stray light might give a significant contribution to these orders, but a precise estimate is not possible because the distribution law of the stray light very close to the central star is unknown, and the actual position of the aperture, which has a 1″ uncertainty, is critical. The 2400 Å discontinuity is present but with decreasing strength in the higher

orders. The saturation does not allow the study the profile of the strong 2750 and 2800 Å emission features. Note the strength of the interstellar Fe II and Mn II blend at 2600 Å. The last order shows a completely different spectrum, which is neither similar to that of η Car, nor to the nebular one. It should be attributed to the faint star, #64 of the Trumpler 16 OB association (Feinstein et al. 1973), which falls near the northern edge of the LWR 9442 image.

Figure 6 shows the line-by-line spectra of the SWP 10778L image. N III] 1750 Å is the dominant emission feature in all the spectra. Bearing in mind the aperture position in Fig. 1, the brightest parts of the S shell fall near the northern part of the aperture (higher spectral orders), where many prominent emission lines are present. The high temperature lines of N V and He II are very strong in the northern orders #28 to #30. These spectra also display intense emissions of the Fe III 1895, 1915, 1926 Å triplet, and the high excitation Fe II lines at 1785–88 Å (UV multiplet 191). The excitation mechanism of the latter in peculiar objects is still unclear, but its presence in a high temperature environment could be suggestive of fluorescent excitation from a high ionization nebular line. But, more probably, the multiplet is excited via dielectronic recombination, as also suggested by the presence of the strong Fe III emission (cf. Johansson & Hansen 1988; Muratorio et al. 1992). Like in the stellar core spectrum, the C III] 1907 Å emission line is absent. Also C IV is undetectable while the C II 1335 Å resonance line is present with a weak emission. These facts, when they are associated with the simultaneous presence of strong emission lines of nitrogen and silicon with similar excitation, seem to suggest a carbon underabundance in the S shell region. It should be important to investigate whether the possible carbon underabundance of the stellar envelope is to be associated with a chemical anomaly of the star, or is, at least partly, the result of the very efficient dust condensation from the stellar wind.

4. Conclusions

The study at high spectral and, possibly, spatial resolution of the diffuse matter ejected by luminous stars is a clue to understand the *LBV* phenomenon, particularly for tracing back their past history. In this regard the nebula surrounding η Car has been and is a source of precious information of the nature of the stellar core. In this paper we have presented and documented dedicated observations of the nebula made in December 1980. In agreement with previous studies (e.g. Davidson et al. 1986) our IUE observations have disclosed the presence of large temperature variation in the circumstellar regions, with higher ionized matter near the X-ray emitting S shell region, and lower temperature regions near the dense NW and SE lobes of the Homunculus. In this paper we have also presented the first high resolution ultraviolet spectrum of the NW region. We have found that the spectrum resembles that of the central star, which indicates a dominant role in that region of the dust scattering of the starlight, as also suggested by the optical observations. The line profiles indicate the presence of a velocity dispersion of up to 1000 km s^{-1}, in agreement with the high velocity features found in the stellar core spectrum (Viotti et al. 1989; Damineli Neto et al. 1993). Of particular interest is the presence of nebular Fe I and Fe II fluorescent lines with a narrow profile. High resolution UV observation of other regions of the Homunculus, especially in the shorter wavelength range, would be of the largest interest to probe the physical and dynamical structure of the ejected material.

Acknowledgements. This work is partly based on data collected from the ULDA database. The research has also benefitted from the use of the SIMBAD database operated at CDS, Strasbourg. We are grateful to M. Friedjung and D.J. Hillier for comments on the manuscript. The extracted spectrograms of the different nebular regions and of η Car, and the line lists of Papers I and II are available from anonymous ftp–server alpha1.ias.fra.cnr.it as ASCII or TEX file in the directory pub/uvspace.

References

Allen D.A. 1989, MNRAS 241, 195
Altamore A., Giangrande A., Viotti R. 1981, A&AS 49, 511
Andriesse C.D., Donn B.D., Viotti R. 1978, MNRAS 185, 771
Burgarella D., Paresce F. 1991, A&A 241, 595
Carpenter K.G., Pesce J.E., Stencel R.E. 1988, ApJS 68, 345
Cassatella A. 1986, Report to the Three Agency Meeting, ESTEC, June 1986, II 13–1
Chlebowski T., Seward F.D., Swank J., Szymkoviak A. 1984, ApJ 281, 665
Damineli Neto A., Viotti R., Baratta G.B., de Araujo F.X. 1993, A&A 268, 183
Damineli Neto A., Viotti R., Cassatella A., Baratta G.B. 1994, Evolution of Massive Stars: a Confrontation between Theory and Observations, eds. D. Vanbeveren, W. van Rensbergen and C. de Loore, Space Sci. Rev. 66, 211
Davidson K., Walborn N.R., Gull T.R. 1982, ApJ 254, L47
Davidson K., Dufour R.J., Walborn N.R., Gull T.R. 1986, ApJ 305, 867
de Boer K.S., Cassatella A. 1986, New Insights in Astrophysics, Proc. Joint NASA/ESA/SERC Conference, ESA SP-263, p. 665
Feinstein A., Marraco H., Muzzio J.C. 1973, A&AS 12, 331
Gaviola E. 1950, ApJ 111, 408
Gaviola E. 1953, ApJ 118, 234
Hester J.J., Light R.M., Westphal J.A. et al. 1991, AJ 102, 654
Hillier D.J., Allen D.A. 1992, A&A 262, 153
Johansson S., Hansen J.E. 1988, Physics of Formation of Fe II Lines Outside LTE, eds. Viotti R. et al., Proc. IAU Coll. 94, (Reidel, Dordrecht) 277
Meaburn J., Wolstencroft R.D., Walsh J.R. 1987, A&A 181, 333

Muratorio G., Viotti R., Friedjung M., Baratta G.B., Rossi C. 1992, A&A 258, 423
Penston M.F. et al. 1983, MNRAS 202, 833
Polcaro V.F., Viotti R. 1993, A&A 274, 807
Ringuelet A.E. 1958, Zs. f. Ap. 46, 276
Thackeray A.D. 1956, The Observatory 76, 154
Thackeray A.D. 1961, Observatory 81, 99
van Genderen A.M., Thé P.S. 1984, Space Sci. Rev. 39, 317
Viotti R. 1968, Mem. Soc. Astr. It. 39, 105
Viotti R., Giangrande A., Cassatella A., Macchetto F. 1981, Space Sci. Rev. 30, 235
Viotti R., Rossi L., Altamore A., Rossi C., Cassatella A. 1986, Luminous Stars and Associations in Galaxies, eds. C.W.H. de Loore, A.J. Willis, P. Laskarides, Proc. IAU Symp. 116 (Reidel, Dordrecht) 249
Viotti R., Cassatella A., Ponz D., Thé P.S. 1988, A&A 190, 333
Viotti R., Rossi L., Cassatella A., Altamore A., Baratta G.B. 1989, ApJS 71, 983 (Paper I)
Walborn N.R. 1976, ApJ 204, L17
Walborn N.R., Blanco V.M. 1988, PASP 100, 797
Walborn N.R., Blanco V.M., Thackeray A.D. 1978, ApJ 219, 498
Whitelock P.A., Feast M.W., Koen C., Roberts G., Carter B.S. MNRAS 270, 364
Whitney C.A. 1952, Harvard College Observatory Bull. 921, 8
Witt A.N., Walker G.A.H., Bohlin R.C., Stecher T.P. 1982, ApJ 261, 492
Zanella R., Wolf B., Stahl O. 1984, A&A 137, 79

Table 2. The ultraviolet spectrum of condensation H of η Car in December 1980 (IUE image No. LWR9453)

BAR WL (1)	A/E (2)	WID (3)	EQW (4)	CONT (5)	ION (6)	LAB WL (7)	REMARKS (8)
2313.9	A	3.9	2.2::	170	NiII	16.03	PCyg *
2343.8	A	9.3	4.6::	175	FeII	43.49, 44.28	PCyg *
					FeII	48.12, 48.30	bl *
2357.9	A	4.7	2.4::	175	FeII	59.11	PCyg *
					FeII	60.00, 60.29	bl *
					FeII	62.02	bl *
2381.6	A	3.9	2.6::	175	FeII	79.27, 80.76	PCyg *
					FeII	82.03, 83.06	bl *
					FeII	84.39	bl *
2382.9	A	1.0	0.6::	117	FeII	82.03	i.s.red
2384.1	E	1.7	0.4::	175	FeII	84.39	? *
2387.1	A	3.9	1.8:	175	FeII	88.63, 91.47	PCyg *
2390.4	E	2.5	1.2::	175	FeII	88.63, 91.47	broad em *
2403.0	A	4.4	1.3::	175	FeII	04.43, 04.88	PCyg *
					FeII	06.66	bl *
2409.4	A	5.4	2.0::	215	FeII	10.52, 11.06	PCyg *
					FeII	13.31	bl *
2417.2	E	6.9	3.1::	250	FeII	18.44?	broad em,fl?
2418.4	E	2.1	1.21:	262	FeII	18.44?	em peak,fl?
					FeIII	18.57?	?
2438.4	E	1.4	0.61:	275	FeII	38.05K	em peak,fl
2439.7	E	1.1	0.42:	275	FeII	39.30	em peak, noisy
2448.3	E	1.0	0.46:	263	FeII	47.32, 47.56	em peak,fl,noisy
2466.2	E	7.5	2.70:	263	FeII	64.90, 65.91	broad em
2493.0	E	5.5	2.22:	268	FeII	91.39, 93.17	broad em
2507.6	E	7.9	8.12	265	FeII	06.80K	broad em,fl*
					FeII	07.59K,07.68K	bl *
					FeII	08.34K	bl *
2507.0	E	1.8	0.97	475	FeII	06.80K	em peak,fl *
2508.5	E	1.1	0.74	475	FeII	08.34K	em peak,fl *
2512.9	E	2.5	1.1::	264	FeII	11.76, 11.91	db?
2529.8	E	2.5	1.65:	263	FeII	29.22, 29.54	em peak
2539.7	E	6.2	3.55:	263	FeII	38.68, 38.90	broad em
2550.9	E	4.0	2.07:	250	FeII	51.28	em peak,fl
2560.2	A	3.2	1.21:	250	FeII	62.53, 63.47	PCyg
2564.2	E	4.4	1.64:	250	FeII	63.47	broad em
2568.6	E	5.5	2.16	250	FeII	66.91	broad em
2573.0	A	2.4	0.93	250	MnII	76.11	PCyg
2576.5	A	0.8	0.32	250	MnII	76.11	i.s.
2579.1	E	4.7	2.30	250	FeII	77.92	broad em
2584.5	A	5.4	2.78	250	FeII	85.88	PCyg
2586.3	A	0.9	0.63	250	FeII	85.88	i.s.,db
2587.1	A	0.4	0.17	250	FeII	85.88	i.s.red
2587.7	E	2.5	0.31	250	FeII	85.88	em peak
2591.0	A	2.6	0.88	250	MnII	93.73	PCyg
2592.7	E	1.5	0.39	250	MnII	93.73	em peak
2594.1	A	0.8	0.33	250	MnII	93.73	i.s.
2599.7	A	1.1	0.74	160	FeII	99.39	i.s.,db
2600.6	A	0.6	0.26	160	FeII	99.39	i.s.red
2601.5	E	2.0	1.16	180	FeII	99.39	em peak *
2604.1	A	2.5	0.68	180	MnII	05.70	PCyg
2606.0	A	1.1	0.30	180	MnII	05.70	i.s.
2607.6	E	2.6	1.56	180	MnII	05.70	em peak
2624.4	E	1.6	0.78	220	FeII	25.66	em peak
2627.3	E	2.1	0.91	220	FeII	28.29	em peak
2632.3	E	8.1	14.88	180	FeII	31.04, 31.32	broad em
2630.4	E	1.7	0.42	480	FeII	31.04, 31.32	em peak
2632.8	E	3.2	1.03	480	FeII	3	em peak
2668.4	E	11.3	6.22:	200	FeII	66.63	broad em

Table 2. continued

BAR WL (1)	A/E (2)	WID (3)	EQW (4)	CONT (5)	ION (6)	LAB WL (7)	REMARKS (8)
					CrII	66.02, 68.71	bl
2693.8	E	2.7	2.01	200	FeII	92.60, 92.83	broad em
2714.9	E	1.2	0.44	390	FeII	14.41	em peak
2716.3	E	1.4	0.32	390	FeII	14.41	red comp *
2716.4	E	6.1	4.31	250	FeII	14.41	broad em
					FeII	16.68	bl
2725.5	E	0.9	0.30	260	FeII	24.88	em peak
2728.7	E	4.0	2.32	290	FeII	27.54	broad em, bl
2728.0	E	0.9	0.19	420	FeII	27.54	em peak
2729.3	E	2.0	0.34	420	FeII	27.54	red comp *
2731.7	E	3.6	2.64	290	FeII	30.73	broad em, bl
2731.3	E	2.2	0.72	420	FeII	30.73	em peak
2733.0	E	0.8	0.09	420	FeII	30.73	red comp *
2740.7	E	8.7	6.06	290	FeII	39.54	broad em
2738.4	E	2.0	1.03	360	FeII	39.54	em peak
2749.7	E	6.2	8.20	290	FeII	49.18,.32,.48	broad em
2756.6	E	7.7	12.06	304	FeII	55.73	broad em
2762.4	E	2.2	0.32	470	FeII	61.81	em peak,db
					CrII	62.58	bl
2767.6	E	2.1	0.79:	330	FeII	68.94	db, bl
2770.2	E	3.7	1.61:	320	FeII	69.35	db, bl
2779.6	E	1.5	0.35:	290	FeII	79.30	noisy
2793.2	A	10.6	6.36	300	MgII	95.52	PCyg +i.s *
2795.9	A	1.7	1.24	110	MgII	95.52	i.s.,db,bl
2796.7	A	0.6	0.45	110	MgII	95.52	i.s.red,bl
2800.1	A	4.9	1.60	310	MgII	02.69	PCyg *
2803.1	A	1.4	0.98	217	MgII	02.69	i.s.,db
2803.9	A	0.6	0.31	217	MgII	02.69	i.s.red
2806.0	E	4.8	7.14	290	MgII	02.69	broad em
2823.0	E	2.3	0.81:	150	FeI	23.28	noisy *
2839.6	E	21.2	18.62	200	FeII	35.72-43.49	broad bl
2836.2	E	1.5	0.39	360	FeII	35.72	em peak,fl
2839.7	E	0.9	0.31	360	FeII	39.53, 39.82	em peak,fl
2844.0	E	1.4	0.39:	360	FeII	43.32, 43.49	em peak,fl
					FeI	43.98?	fl *
2845.7	E	1.3	0.71	360	FeII	45.60K	em peak,fl
2850.7	E	1.0	0.31	350	FeII	50.64	mult,fl
2851.7	E	0.8	0.17	350	FeII	51.74	em peak fl
2852.6	A	1.0	0.60	350	MgI	52.12	i.s.
2853.5	A	0.6	0.14	350	MgI	52.12	i.s.red
2856.9	E	2.1	0.45	350	FeII	56.93, 57.17	em peak,fl
2881.6	E	1.9	0.59:	313			em peak,db *
2908.2	E	7.5	4.73	170	FeII	07.85, ...	broad em,db,neb
2916.5	E	3.5	1.38	160	FeII	16.15	
2927.3	E	10.9	12.78	200	FeII	26.58	broad em
2927.1	E	3.7	1.23	450	FeII	26.58	em peak
2930.8	A	1.9	0.36	420			RM ??
2938.1	E	1.9	0.95	240			em peak,eta *
2939.9	E	1.6	0.95	240	FeII	39.51	em peak
2944.5	E	1.9	0.66	250	FeII	44.40	em peak
2952.5	E	11.9	11.85	240	FeII	47.66,49.18	broad em
					FeII	53.77	bl
2948.2	E	1.7	0.63	340	FeII	47.66	em peak
2949.8	E	1.7	0.67	340	FeII	49.18	em peak
2954.1	E	2.5	1.02	450	FeII	53.77	em peak
2965.4	E	2.9	1.28	275	FeII	64.62, 65.04	em peak,RM
2971.2	E	5.8	3.33	275	FeII	69.93	broad em
2970.8	E	2.2	0.70	400	FeII	69.93	em peak
2976.0	E	1.6	0.46	240			em peak,eta
2979.7	E	3.5	1.61	240	FeII	79.35	m

Table 2. continued

BAR WL (1)	A/E (2)	WID (3)	EQW (4)	CONT (5)	ION (6)	LAB WL (7)	REMARKS (8)
2986.2	E	8.4	6.63	240	FeII	84.83, 85.54	broad em
2986.2	E	3.5	0.73	450	FeII	85.54	em peak
3003.5	E	7.9	6.49:	170	FeII	02.65	broad em
3003.3	E	3.6	2.23	225	FeII	02.65	em peak
3020.2	E	1.3	0.92::	125			em peak,noisy
3077.2	E	2.5	3.15:	160	FeII	76.45, 77.17	bl
3091.9	E	2.7	1.4::	170			em peak,noisy
3161.9	E	4.5	2.3::	250	FeII	61.95	noisy
3196.2	E	6.9	6.7::	250	FeII	92.92, 93.81	broad em,noisy
					FeII	96.07	bl
3195.7	E	3.9	2.1::	380	FeII	92.92, 93.81	em peak,noisy
3228.0	E	1.2	1.1::	420	FeII	27.73	em peak,noisy

Notes to the table:

2313-2409: This region is difficult to analyze for the low S/N and the crowding of the lines.

2714.9: Red shifted emission peak probably present in other FeII lines, but measurable only in a few cases.

2800.1: Area between two peaks which are the residual of the broad blend of the red emission wing and of the blue emission wing of Mg II 2795 e 2803, respectively.

2823.0: This line, which is also present in the stellar core spectrum, is attributed to FeI 2823.28 excited by fluorescence by the Mg II h line. The other fluorescence line at 2843.98 A is blended with an Fe II line.

2881.6: Many weak emission features are present in this region which are too noisy to be measured.

2938.1: Stronger in nebular spectrum. Possibly Mg II 2936.50.